Journal of Biomechanics 96 (2019) 109336

Contents lists available at ScienceDirect

Journal of Biomechanics

journal homepage: www.elsevier.com/locate/jbiomech
www.JBiomech.com

On the fracture mechanisms of nacre: Effects of structural orientation

D. Jiao [a], R.T. Qu [a,b], Z.Y. Weng [a], Z.Q. Liu [a,b,*], Z.F. Zhang [a,b,*]

[a] Laboratory of Fatigue and Fracture for Materials, Institute of Metal Research, Chinese Academy of Sciences, Shenyang 110016, China
[b] School of Materials Science and Engineering, University of Science and Technology of China, Hefei 230026, China

ARTICLE INFO

Article history:
Accepted 8 September 2019

Keywords:
Fracture
Lamellar structure
Structural orientation
Nacre
Biomechanics

ABSTRACT

The nacre of mollusk shells is distinguished by an exceptional mechanical efficiency which is derived essentially from its lamellar structure and frequently acts as a source of inspiration for the development of biomimetic materials. The structure and mechanical properties of nacre have been intensively investigated with a special focus on its toughening strategies; nevertheless, the fracture mechanisms, more specifically the critical stress/strain conditions for the failure of nacre, and the effects of structural orientation and hydration state remain largely unexplored. Here uniaxial compression tests were performed on nacre of both dry and hydrated states with different off-axis angles, *i.e.*, the inclination of loading axis with respect to the lamellar structure, ranging from 0° to 90°. The mechanical properties and fracture characteristics of nacre and their dependences on the structural orientation and hydration state were elucidated in terms of mechanics behind failure. Quantitative relationships were established between the mechanical properties and off-axis angle based on different failure criteria. The competition between the fracture modes of fragmentation and shearing was quantified by comparing their respective driving force and resistance on the interfacial plane. This study may aid the understanding on the mechanical behavior of nacre and nacre-inspired synthetic materials and promote a better replication of the underlying design principles of nacre in man-made systems.

1. Introduction

Natural organisms are adept at synthesizing high-performance materials using a simple palette of constituents comprising mainly weak bio-polymers and brittle bio-minerals under relatively mild conditions (Meyers et al., 2008a, 2013; Dunlop and Fratzl, 2010; Liu et al., 2017; Naleway et al., 2015). The resulting materials usually exhibit outstanding mechanical properties, especially as compared to their constituents, demonstrating an exceptional mechanical efficiency of design (Bar-On and Wagner, 2012; Ritchie, 2011; Ji, 2008; Li and Ortiz, 2013; Li et al., 2015). This results essentially from their intricate structures which have been optimized through the long-term evolution process (Meyers et al., 2008a). An excellent case in point is the nacre which generally forms in the inner layer of mollusk shells (Barthelat, 2010; Sun and Bhushan, 2012). It consists mainly of aragonite minerals (~95 vol%) – an orthorhombic crystalline form of calcium carbonate, and a minor content of organic matter. The aragonite (*e.g.*, in the nacre of red abalone shell) typically has a polygonal platelet geometry which is 5–10 μm in width and ~0.5 μm in thickness (Song and Bai, 2003; Li et al., 2004). These mineral platelets are piled up in a lamellar fashion with the interfaces between them occupied by organic matter, forming the so-called "brick-and-mortar" architecture.

The ingenious structural design endows nacre with a remarkable synergy of strength and fracture toughness. In particular, it enables the activation of a series of toughening mechanisms in nacre, including the inelastic shearing of organic layer (Barthelat et al., 2007; Smith et al., 1999), crack deflection along interfaces (Dastjerdi et al., 2013; Menig et al., 2000), crack bridging via "pull-out" of mineral platelets (Dastjerdi et al., 2013; Lin and Meyers, 2009), and platelet interlocking during sliding (Barthelat et al., 2007; Barthelat and Espinosa, 2007). This provides for an increase of fracture toughness by a factor of over three orders of magnitude (in energy terms) compared to simple mixture of constituents (Barthelat, 2010). As such, nacre has been frequently regarded as a natural model in terms of biomimetics and bioinspiration (Bouville et al., 2014; Munch et al., 2008; Deville et al., 2006). The implementation of the design principles extracted from nacre offers an effective means for achieving improved mechanical properties in man-made materials. One prime example is a hybrid

* Corresponding authors at: Laboratory of Fatigue and Fracture for Materials, Institute of Metal Research, Chinese Academy of Sciences, Shenyang 110016, China.
E-mail addresses: zengqianliu@imr.ac.cn (Z.Q. Liu), zhfzhang@imr.ac.cn (Z.F. Zhang).

https://doi.org/10.1016/j.jbiomech.2019.109336
0021-9290/

composite made of laminated glass tablets infiltrated with an elastomer (ethylene-vinyl acetate) as a compliant phase (Yin et al., 2019). The replication of nacre's three-dimensional "brick-and-mortar" architecture endows such material with exceptional impact resistance that is two times higher than tempered glass while maintaining high stiffness and strength.

Any success in the design of nacre-like materials rests on a deep understanding about the mechanical behavior of nacre *per se*. The structure and mechanical properties of nacre have been intensively explored with a special effort made to unravel its toughening strategies (Barthelat et al., 2006; Espinosa et al., 2011; Yourdkhani et al., 2011). Menig *et al.* investigated the fracture behavior of nacre in abalone shell under compressive load along the directions parallel and perpendicular to its lamellar structure (Menig et al., 2000). The orientation that is inclined by 45° with respect to the loading axis was examined by Barthelat *et al.* (Barthelat et al., 2007). In addition, several micro- and nano-scale structural characteristics, such as the nano-asperities, bridges, and wavy geometry of mineral tablets, of nacre have been identified; the roles they play in enhancing the mechanical properties have also been clarified (Barthelat et al., 2006; Evans et al., 2001; Wang et al., 2001). In general, the deformation and fracture of nacre have been revealed to be mediated primarily by the viscoplastic shearing of interfacial organic matter between aragonite platelets (Lin and Meyers, 2009; Xu and Li, 2011; Zheng et al., 2018). Nevertheless, the fracture mechanisms, more specifically the critical stress/strain conditions for the failure of nacre, and the effects of structural orientation and hydration state still remain largely unexplored. There is still a lack of systematic and quantitative mechanistic understanding on the fracture of nacre and nacre-mimetic materials.

Here the mechanical properties and fracture behavior of nacre at both dry and hydrated states were examined for a series of off-axis angles, *i.e.*, the inclination of loading axis with respect to the lamellar structure. The orientation-dependence of strength was analyzed by employing different failure criteria. The fracture mechanisms were explored with the competition between differing mechanisms evaluated from a mechanistic perspective. Our approach is supposed to be applicable to other biological materials and nacre-mimetic materials with lamellar structure.

2. Materials and methods

Air-dried shells in thickness of ~6 mm of adult *Sinanodonta woodiana* mollusk (Bivalvia: Unionidae) were obtained from an online store. The external dark brown layers of the shells have been removed by milling at the as-received state, leaving only the nacreous layers with visible growth lines, as shown in Fig. 1(a). For microstructural characterization, a piece of nacre was excised from the shell and manually bent to fracture. The fracture surface was sputter-coated with a thin film of gold and then examined by field emission scanning electron microscopy (SEM) using an LEO Supra 55 instrument operating at an accelerating voltage of 10 kV. The structure was additionally probed using field emission transmission electron microscopy (TEM) on an FEI Tecnai G2 F20 system. The observation was conducted with the incident electron beam nearly parallel and perpendicular to the lamellar structure of nacre. A detailed description about the preparation and characterization of TEM samples can be found in our previous studies (Jiao et al., 2015, 2016a).

Rectangular specimens in dimensions of $2 \times 2 \times 4\ mm^3$ were used for uniaxial compression test. The inclination of the loading axis (the loading is along the height direction of sample) with respect to the lamellar structure of nacre is termed the off-axis angle γ, as illustrated in Fig. 2(a). Samples with a series of off-axis angles ranging from 0° to 90°, *i.e.*, 0°, 15°, 30°, 45°, 60°, 75° and 90°, were excised from the nacre using a low-speed diamond

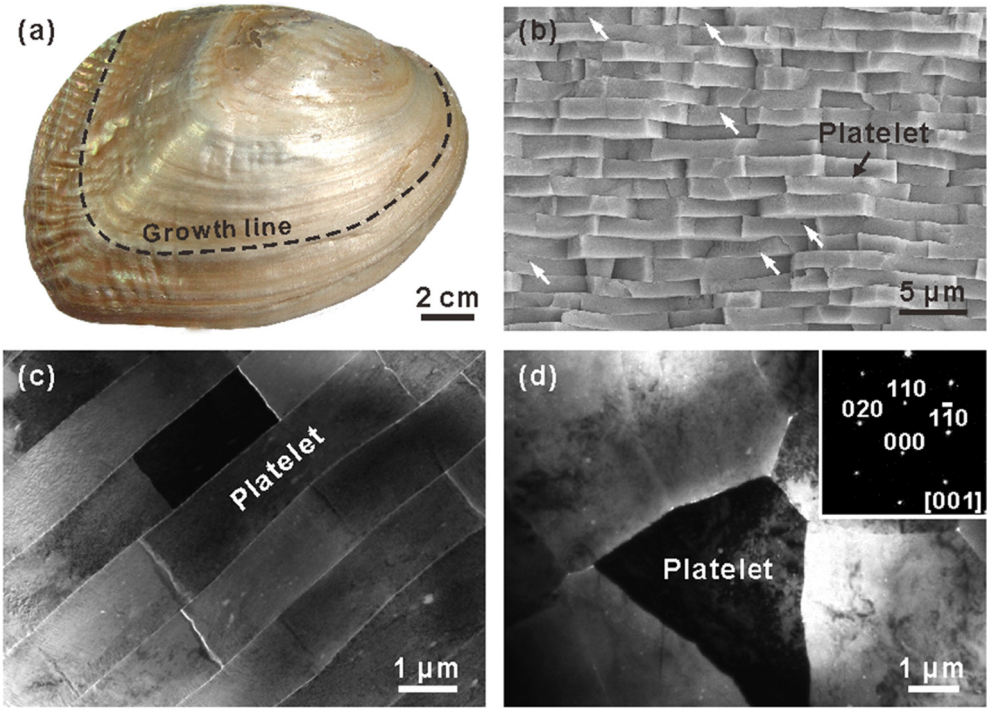

Fig. 1. (a) Macroscopic appearance of a *Sinanodonta woodiana* shell. The dashed curve indicates a growth line on the shell. (b) SEM micrograph of the cross-section of nacre in *Sinanodonta woodiana* shell. The white arrows indicate the structural flaws within the mineral platelets. (c, d) Bright-field TEM micrographs of the aragonite platelets in nacre with the electron beam nearly parallel (c) and perpendicular (d) to the lamellar structure. The inset in (d) shows the corresponding selected area electron diffraction pattern of the platelet.

wire saw (STX-202A, Kejing Auto-Instrument Co., Ltd, China) equipped with a diamond-coated stainless wire with diameter of 0.3 mm. A low cutting speed of 0.1 mm/min was used with the nacre continuously irrigated with water for cooling to minimize damage of samples introduced by the cutting process. Such procedure was proved to have no significant influence on the strength of nacre as compared to the carefully polished specimens by removing the surface layers of saw-cut samples (see Supplementary Materials). Rehydration of nacre was realized by immersing samples in water for ten days. This was revealed to result in a stable hydrated state of nacre by analyzing the variation of water content during the hydration process (see Fig. S1 in Supplementary Materials). The water contents of air-dried and rehydrated samples were determined to be 0.07 wt% and 0.58 wt%, respectively.

Uniaxial compression test was performed on samples of both air-dried and hydrated states at a constant strain rate of 10^{-4} s^{-1} at room temperature using an Instron 8871 testing system. At least four samples were tested for each orientation and each hydration state. The differences in mechanical properties were statistically tested using two-tailed Student's *t*-test at a significance level of 0.05. The normality of distribution of strength data has been validated using the Shapiro-Wilk testing method (see Supplementary Materials). The lateral and fracture surfaces of samples after compression were sputter-coated with gold and observed by SEM.

3. Results and discussion

The macroscopic appearance and microstructure of the nacre from *Sinanodonta woodiana* shell are shown in Fig. 1. Polygonal-shaped aragonite platelets are arranged in parallel and densely packed in the nacre. These platelets have a thickness of 0.3–1.7 μm and display a crystal orientation with their [0 0 1] axis normal to lamellae. The lamellae are aligned nearly orthogonal to the thickness direction of shell. Such structure is essentially similar to that of nacre from other mollusks (Barthelat, 2010; Chen et al., 2008; Meyers et al., 2008a). Careful examination reveals the existence of flaws (*e.g.*, pores) within the mineral platelets of nacre, as indicated by the white arrows. Similar structural imperfections of differing length-scales have also been detected in other mollusk shells (Barthelat and Espinosa, 2007; Gries et al., 2009; Jiao et al, 2015; Schaffer et al., 1997), and may have an effect on the mechanical properties and failure behavior of nacre (as will be discussed later). The *Sinanodonta woodiana* shell has a comparatively thick nacreous layer that exceeds 5 mm. This enables the excision of samples with arbitrary structural orientation from it for compression test.

Fig. 2 shows the compressive mechanical properties of nacre with different off-axis angles at dry and hydrated states. Note that the stress-strain curves have been horizontally shifted for clarity. Detailed results of statistical analysis are presented in Table S1 in the Supplementary Materials. The mechanical properties of nacre, including the compressive strength, failure strain and work-of-fracture (represented by the area under the stress-strain curve), demonstrate a clear dependence on the off-axis angle. A general varying trend for both hydration states is that the strength and work-of-fracture decrease with increasing off-axis angle, reach the minima at 30–45° orientation, and then increase until the loading direction is perpendicular to lamellar structure. The sample with 45° off-axis angle displays significantly lower strength compared to near longitudinal (0°) and orthogonal (90°) directions.

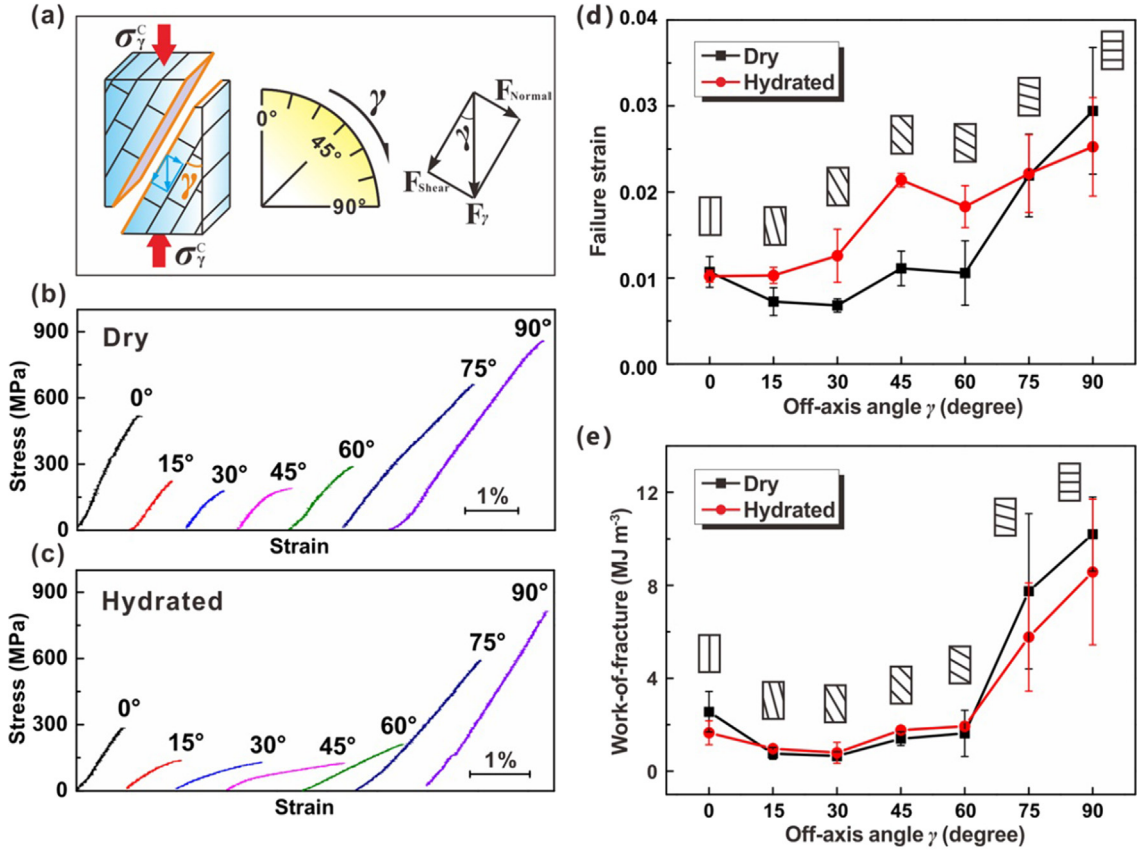

Fig. 2. (a) Schematic illustrations of the inclination of loading axis with respect to the lamellar structure of nacre and the resolution of compressive force on the interfacial plane. (b, c) Typical compressive stress-strain curves of nacre with different off-axis angles at (b) dry and (c) hydrated states. (d, e) Variations of the (d) compressive failure strain and (e) work-of-fracture with the off-axis angle of nacre at dry and hydrated states.

Nevertheless, this orientation is featured by an apparent plasticity and a marked increase of failure strain at both dry and hydrated states. This is supposed to result from the easy interfacial shear at such configuration where the resolved shear stress presents a maximum on the lamellar interface.

Hydration tends to decrease the strength of nacre for the 45° off-axis angle and near longitudinal directions (0–15°). However, the nacre displays a significant enhancement of deformation capability at the hydrated state at the range of off-axis angles from 15° to 60°. The strength, failure strain and work-of-fracture of nacre at both hydration states demonstrate the maxima at 90° off-axis angle, suggesting the achievement of the best combinations of mechanical properties when the lamellar structure is perpendicular to loading direction. This is exactly the actual structural orientation of nacre in accomplishing its biomechanical functionality as an armor, *e.g.*, by resisting a biting or striking force. Nevertheless, the mechanical properties of nacre at such orientation exhibit a large scatter which is supposed to result from the existence of structural flaws (Fig. 1).

Representative fracture morphologies of air-dried nacre with different off-axis angles are shown in Fig. 3. Typical morphologies of hydrated samples are shown in Fig. S2 in Supplementary Materials. The macroscopic fracture mode and microscopic fracture mechanisms of nacre at both hydration states are closely associated with the loading direction. The nacre with 0° off-axis angle, *i.e.*, the compressive load is parallel to lamellar structure, fails mainly by vertical splitting and tends to rupture into small blocks (Fig. 3(a) and Fig. S2(a)). Such mode is principally characterized by inter-lamellar cracking at the micro-level. The fracture of nacre with off-axis angles of 15–60° occurs mainly by inter-lamellar shearing which leads to a straight fracture plane right along the interface of lamellar structure (Fig. 3(b) and Fig. S2(b)). The fracture profile may shift among adjacent interfaces between lamellae at the micro-scale, resulting in tiny steps on the fracture surface. The nacre displays a fracture mode of trans-lamellar fragmentation at 90° off-axis angle where the compressive load is along the orthogonal direction of lamellar structure (Fig. 3(d) and Fig. S2 (d)). The cracks propagate largely across the aragonite platelets in this mode as can be indicated by the fragmented mineral pieces on the fracture surface, which contrasts to the inter-lamellar splitting at 0° off-axis angle. Such trans-platelet fracture of mineral platelets is supposed to be more sensitive to the flaws existing within platelets as compared to the interfacial fracture for other orientations, thus leading to a large scatter of mechanical properties. Indeed, nano-scale pores with a random distribution can be observed on the fracture surface of nacre at this loading direction (see Fig. S3 in Supplementary Materials). For the 75° off-axis angle, the nacre exhibits a mixed fracture mode of fragmentation and inter-lamellar shearing (Fig. 3(c) and Fig. S2(c)). The above morphological features at each fixed off-axis angle remain similar between dry and hydrated states, as seen in Fig. 3 and Fig. S2; this suggests that the structural orientation plays a dominant role in determining the fracture mechanisms of nacre as compared to hydration state.

For the failure modes of shearing and splitting, the fracture of nacre is essentially caused by cracking along the interfaces between lamellae, leading to a good consistency of the main fracture profile with interfacial plane. Under uniaxial compression, the nominal compressive stress, σ_γ, for off-axis angle γ can be resolved to a shear stress τ and a normal stress σ which is, respectively, parallel and perpendicular to the interfacial plane. The resolved stresses can be described as a function of the off-axis angle γ as:

$$\sigma = \sigma_\gamma \sin^2 \gamma \tag{1}$$

and

$$\tau = \sigma_\gamma \sin \gamma \cos \gamma \tag{2}$$

It has been revealed that the off-axis strength of unidirectional laminates, such as the glass-fiber reinforced composites plates, can frequently be captured by the Tsai-Hill failure criterion which has the following form:

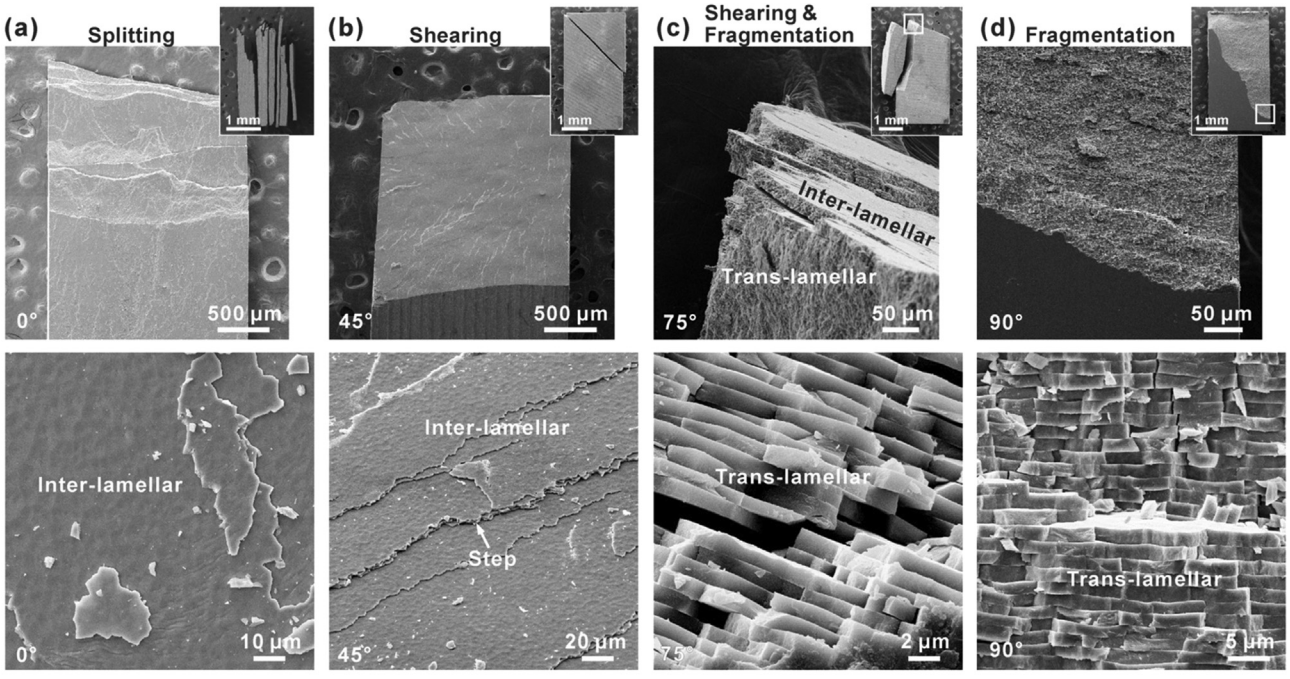

Fig. 3. Representative SEM micrographs of the fractured nacre with off-axis angles of (a) 0°, (b) 45°, (c) 75°and (d) 90° at the dry state. The upper right insets show the macroscopic lateral view of the samples. The upper left images in (c) and (d) present the magnified view of the circled regions in the insets. The lower images show the magnified morphologies of the fracture surfaces.

$$\sigma_\gamma^C = \left[\cos^4\gamma/X^2 - \cos^2\gamma\sin^2\gamma/X^2 + \sin^4\gamma/Y^2 + \sin^2\gamma\cos^2\gamma/S^2\right]^{-1/2} \quad (3)$$

where σ_γ^C depicts the compressive strength at given off-axis angle γ, X and Y represent the strengths along the longitudinal and orthogonal directions, and S is the shear strength (Azzi and Tsai, 1965; Hill, 1965; Tsai, 1968). Here this criterion has been applied to nacre in elucidating the orientation-dependence of compressive strength. As shown in Fig. 4, the Tsai-Hill failure criterion offers a rough description about the general varying trend of strength over the entire orientation range; however, it demonstrates a relatively low goodness-of-fit, especially for the 15–75° off-axis angles where shearing occurs.

In light of the strength variation of nacre with off-axis angles exhibiting shearing fracture mode, the Tresca failure criterion (Tresca, 1864), or termed the maximum shear stress criterion, has been applied to the range of 15–75°. Based on this criterion, the failure of materials occurs when the resolved shear stress at any plane (specifically the interfacial plane in the present case) reaches a critical level. Additionally, the Drucker-Prager failure criterion which describes the pressure-dependent yielding behavior of materials (Drucker and Prager, 1952), such as rock, has also been employed in analysis. According to this criterion, the critical stress conditions for failure can be described as:

$$\tau = \sqrt{2/3}(3\lambda\sigma + \kappa) \quad (4)$$

where λ and κ are material constants. Moreover, a generalized failure criterion, also termed the ellipse criterion, has been developed for describing the shearing fracture of materials based on a critical energy density that can be stored in materials (Zhang and Eckert, 2005; Qu and Zhang, 2013; Qu et al., 2016). Such criterion also presents a good applicability to materials where the shearing behavior demonstrates a dependence on normal stress. According to the ellipse criterion, the critical stress conditions for shearing fracture can be described as:

$$(\tau/\tau_0)^2 + \beta(\sigma/\sigma_0)^2 = 1 \quad (5)$$

where β is a parameter associated with stress state (Qu and Zhang, 2013; Qu et al., 2016). The parameters τ_0 and σ_0 reflect the inherent resistance of shearing plane, *i.e.*, the interfacial plane in the case of nacre, against failure caused merely by shear stress and normal stress, respectively. It is noted that σ_0 is not necessarily consistent with the strength of nacre at 90° off-axis angle where trans-lamellar and trans-platelet fracture occurs (instead of the interfacial failure). Accordingly, the nominal compressive strength σ_γ^C can be correlated to the off-axis angle γ as:

$$\sigma_\gamma^C = \sigma_0\tau_0/\left(\sin\gamma\sqrt{\left(\sigma_0^2\cos^2\gamma + \beta\tau_0^2\sin^2\gamma\right)}\right) \quad (6)$$

It is noted that the Tresca, Drucker-Prager and ellipse failure criteria are applicable to materials where the failure or fracture is dominated by shearing mode. As such, these criteria have only been employed to analyze the off-axis angles of 15–75° in this study. As shown in Fig. 4(a) and (b), both the Drucker-Prager and ellipse failure criteria give a good description about the critical stress conditions for the fracture mode of inter-lamellar shearing of nacre at both dry and hydrated states. These criteria are not

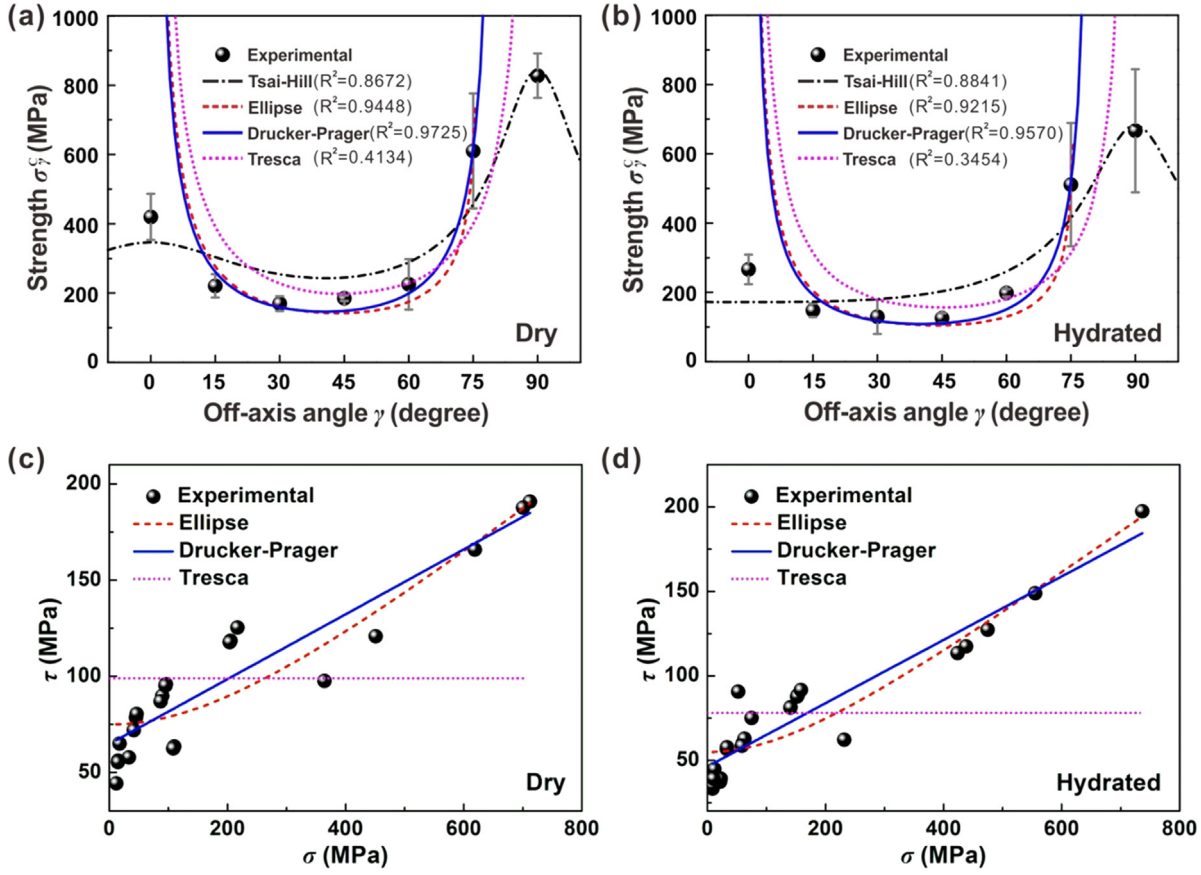

Fig. 4. (a, b) Compressive strength of nacre as a function of the off-axis angle at (a) dry and (b) hydrated states and fitting results using different failure criteria. The Tresca, Drucker-Prager and ellipse criteria were applied only for the 15–75° off-axis angles where shearing fracture occurs. (c, d) Critical combinations of resolved shear stress τ and normal stressσ on the interfacial plane of nacre for fracture at (c) dry and (d) hydrated states for the 15–75° off-axis angles.

applicable to the 0° and 90° off-axis angles where splitting and fragmentation occur instead of shearing. Despite a relatively lower goodness-of-fit than the Drucker-Prager criterion, the ellipse criterion offers a direct evaluation about the intrinsic properties of the lamellar interface in nacre. The resolved shear stress on the fracture plane of nacre demonstrates an increasing trend with the increase of resolved normal stress, as shown in Fig. 4(c) and (d). This suggests a role of resolved compressive stress in resisting the shearing fracture of nacre, *e.g.*, by increasing the interfacial friction between adjacent lamellae.

The parameters τ_0 and σ_0 were fitted to be 69 MPa and 197 MPa for air-dried nacre following the ellipse failure criterion. Hydration results in a decrease of τ_0 and σ_0 by ~25.8% and ~22.5%, respectively, to 51 MPa and 153 MPa. The strength of the pure organics at interfaces between lamellae at hydrated state has been determined to be 0.6–1.5 MPa by tension test on demineralized nacre (Dastjerdi et al., 2013; Meyers et al., 2009; Lopez et al., 2014). The organics display even lower strength at decreasing strain rates (Lopez et al., 2014). Molecular pull test has revealed large extensibility and "saw-tooth" like pattern in the force-extension curves of interfacial organics, which result from the breakage of sacrificial length or unfolding of hidden length (Lopez et al., 2014, 2016). In comparison, the present results indicate that the interfaces in nacre are much stronger than organics but display limited deformability. The shear strength of interfaces in nacre has been measured experimentally by shear test to be 60–70 MPa and 40–60 MPa, respectively, for dry and hydrated states (Barthelat et al., 2007; Evans et al., 2001; Lin and Meyers, 2009). These values are well consistent with our analysis, suggesting a significant strengthening effect of the interfaces as compared to pure organics.

The enhanced interfacial strength of nacre can be attributed to several micro-/nano- structural characteristics. Firstly, the wavy nature of mineral platelets at the micro-scale, as can be seen in Fig. 1(c), results in the interlocking between platelets during their mutual sliding and generates an expansion in the region of deformation (Barthelat et al., 2007; Barthelat and Espinosa, 2007). Secondly, the mineral platelets are decorated with abundant nano-asperities and interconnected with nano-scale mineral bridges (Evans et al., 2001; Wang et al., 2001; Song and Bai, 2003; Song et al., 2003). These nanostructures act to reinforce the interfaces and resist the inter-lamellar shearing by increasing the interfacial roughness and friction. Thirdly, the lamellae of nacre are usually not well-defined, but are intersected via screw dislocation-like connection centers (Li and Ortiz, 2015; Lin et al., 2008; Yao et al., 2009). Such structure is believed to provide a biomineralization pathway for the formation of nacre through the spiral growth mechanism (Li and Ortiz, 2015; Yao et al., 2009). It has been proved to play an additional role in increasing the resistance for delamination and interfacial sliding through enhanced interlocking (Barthelat et al., 2007; Barthelat and Espinosa, 2007).

It is noted that the mechanical properties of pure organics in biological materials generally demonstrate a strong dependence on the moisture content (Lopez et al., 2014; Liu et al., 2015, 2016). The interfacial organics in nacre, which comprise primarily chitinous nanofibrils embedded within a proteinaceous matrix, have been revealed to display a low modulus but a large extensibility at hydrated state (Lopez et al., 2014; Meyers et al., 2008b). Dehydration plays a significant role in stiffening and hardening these organics, but markedly decreases their extensibility (Barthelat and Espinosa, 2007). However, the interfacial shear strength here presents a moderate decrease in hydrated nacre as compared to dry state; this also contrasts to the extreme softening of pure organics by hydration. Such reduced effects of hydration are also closely associated with the above interfacial strengthening and stabilizing mechanisms. These mechanisms originate essentially from the micro-/nano- interfacial structures between mineral platelets and thus present a low sensitivity to the moisture content.

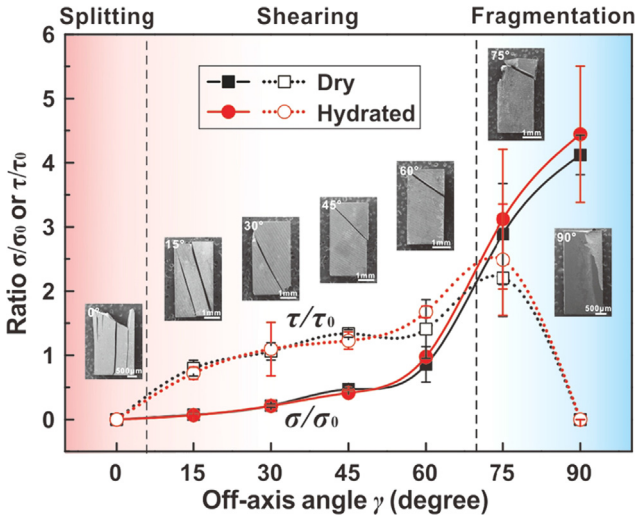

Fig. 5. Evaluation of the competition between the fracture mechanisms of shearing and fragmentation in nacre using the ratio between the resolved interfacial stresses and corresponding resistances of τ/τ_0 and σ/σ_0. Representative lateral morphologies of fractured nacre with different off-axis angles are shown in the insets.

The fragmentation fracture near the orthogonal orientation (*i.e.*, 90° off-axis angle) and the shearing fracture at 15–75° of nacre are primarily associated with the resolved normal stress and shear stress on the interfacial plane, respectively. The competition between the two modes can be evaluated by comparing the resolved stresses, which act as the driving force, with corresponding resistances of the interface. The relative relationship between τ/τ_0 and σ/σ_0 offers a prime assessment for the fracture tendency of shearing or fragmentation of nacre. As shown in Fig. 5, τ/τ_0 and σ/σ_0 play a dominant role at the off-axis angles of 15–60° and 90°, respectively, for both dry and hydrated states, conforming well to the fracture modes of shearing and fragmentation of nacre. The decreasing component of interfacial shear stress towards the orthogonal orientation results in a transition of failure mode from shearing to fragmentation. Such transition occurs around the 75° off-axis angle where τ/τ_0 and σ/σ_0 approximate. This corresponds exactly to the mixed-mode fracture of fragmentation and shearing in nacre.

In terms of the longitudinal orientation, the applied compressive load, which is parallel to the lamellar structure of nacre, creates lateral expansion and local tensile stress at the interfaces (Ashby and Hallam, 1986; Sammis and Ashby, 1986; Wang et al., 1995). This leads to the formation and linkage of micro-cracks along the interfaces and eventually results in the fracture of nacre by means of splitting. Such failure is associated with multiple factors like the interfacial stress concentrations and stability of lamellae, and thus cannot be directly assessed using the resolved interfacial stresses following the above analysis. The mechanical instability (*e.g.*, buckling) generally tends to promote the splitting failure of laminates and thus decrease their strength (Jones, 1999; Liu et al., 2019). This seems to be also the case for nacre where micro-buckling has been observed under compression (Jiao et al., 2016b; Lin et al., 2006; Menig et al., 2000).

4. Conclusions

As a natural model for biomimicry, nacre exhibits an exceptional mechanical efficiency which is derived from its architectural designs. The aragonite platelets are arranged in a lamellar fashion

with the interfaces between them filled with a minor content of organics. Such structure leads to markedly varying strength and fracture behavior of nacre depending on its structural orientation with respect to loading axis. Here the fracture mechanisms of nacre were clarified through a systematic investigation of its compressive properties with differing off-axis angles at both dry and hydrated states. The strength, failure strain and work-of-fracture were revealed to demonstrate clear dependences on the off-axis angle with the best combinations of mechanical properties generated at the orthogonal orientation where the load is perpendicular to lamellar structure. The nacre fractures by axial splitting as is loaded along its lamellar structure and displays inter-lamellar shearing as the load is inclined by 15–60° with respect to structure. Trans-lamellar fragmentation and trans-platelet fracture of mineral platelets occur at the orthogonal orientation with the fracture at 75° off-axis angle featured by mixed mode of fragmentation and shearing. The orientation-dependence of strength was clarified by employing different failure criteria with the failure mode evaluated in terms of the competition between shearing and fragmentation.

The highest strength of general laminated engineering composites is frequently generated at the longitudinal orientation, *i.e.*, along the long axis of fibers or laminates. In comparison, the strength of nacre demonstrates an orientation dependence that cannot be well captured by the Tsai-Hill failure criterion, and displays a maximum at the orthogonal direction which is exactly the configuration as it functions. Additionally, the interfaces in nacre are proved to be markedly strengthened and less sensitive to hydration as compared to its major component – the organics. This results from the micro-/nano- structural characteristics of interfaces which may guide the interfacial design of man-made composites. We expect that the current analysis may be applicable to other biological materials with lamellar structure and synthetic materials mimicking nacre. The refinement of the fracture modes and mechanisms could also aid the understanding about the designs of nacre which could be translated into man-made systems.

Acknowledgements

The authors are grateful to Dr. Q.Q. Duan and X.G. Wang for technical assistance in mechanical testing. This work was financially supported by the National Natural Science Foundation of China (Grant Nos. 51871216 and 51501190).

Declaration of Competing Interest

The authors declare no conflict of interest.

Appendix A. Supplementary material

Supplementary data to this article can be found online at https://doi.org/10.1016/j.jbiomech.2019.109336.

References

Ashby, M.F., Hallam, S.D., 1986. The failure of brittle solids containing small cracks under compressive stress states. Acta Metall. 34, 497–510.
Azzi, V.D., Tsai, S.W., 1965. Anisotropic strength of composites. Exp. Mech. 5, 283–288.
Barthelat, F., Li, C.M., Comi, C., Espinosa, H.D., 2006. Mechanical properties of nacre constituents and their impact on mechanical performance. J. Mater. Res. 21, 1977–1986.
Barthelat, F., Tang, H., Zavattieri, P.D., Li, C.M., Espinosa, H.D., 2007. On the mechanics of mother-of-pearl: a key feature in the material hierarchical structure. J. Mech. Phys. Solids 55, 306–337.
Barthelat, F., Espinosa, H.D., 2007. An experimental investigation of deformation and fracture of nacre–mother of pearl. Exp. Mech. 47, 311–324.
Barthelat, F., 2010. Nacre from mollusk shells: a model for high-performance structural materials. Bioinspiration Biomimetics 5, 35001.
Bar-On, B., Wagner, H.D., 2012. Elastic modulus of hard tissues. J. Biomech. 45, 672–678.
Bouville, F., Maire, E., Meille, S., Van de Moortèle, B., Stevenson, A.J., Deville, S., 2014. Strong, tough and stiff bioinspired ceramics from brittle constituents. Nat. Mater. 13, 508–514.
Chen, P.-Y., Lin, A.Y.M., Lin, Y.S., Seki, Y., Stokes, A.G., Peyras, J., Olevsky, E.A., Meyers, M.A., McKittrick, J., 2008. Structure and mechanical properties of selected biological materials. J. Mech. Behav. Biomed. Mater. 1, 208–226.
Dastjerdi, A.K., Rabiei, R., Barthelat, F., 2013. The weak interfaces within tough natural composites: experiments on three types of nacre. J. Mech. Behav. Biomed. Mater. 19, 50–60.
Deville, S., Saiz, E., Nalla, R.K., Tomsia, A.P., 2006. Freezing as a path to build complex composites. Science 311, 515–518.
Drucker, D.C., Prager, W., 1952. Soil mechanics and plastic analysis or limit design. Q. Appl. Math. 10, 157–165.
Dunlop, J.W., Fratzl, P., 2010. Biological composites. Annu. Rev. Mater. Res. 40, 1–24.
Espinosa, H.D., Juster, A.L., Latourte, F.J., Loh, O.Y., Gregoire, D., Zavattieri, P.D., 2011. Tablet-level origin of toughening in abalone shells and translation to synthetic composite materials. Nat. Commun. 2, 173.
Evans, A.G., Suo, Z., Wang, R.Z., Aksay, I.A., He, M.Y., Hutchinson, J.W., 2001. Model for the robust mechanical behavior of nacre. J. Mater. Res. 16, 2475–2484.
Gries, K., Kroger, R., Kubel, C., Fritz, M., Rosenauer, A., 2009. Investigations of voids in the aragonite platelets of nacre. Acta Biomater. 5, 3038–3044.
Hill, R., 1965. Theory of mechanical properties of fiber-strengthened materials-III. self-consistent model. J. Mech. Phys. Solids 13, 189–198.
Ji, B., 2008. A study of the interface strength between protein and mineral in biological materials. J. Biomech. 41, 259–266.
Jiao, D., Liu, Z.Q., Zhang, Z.J., Zhang, Z.F., 2015. Intrinsic hierarchical structural imperfections in a natural ceramic of bivalve shell with distinctly graded properties. Sci. Rep. 5, 12418.
Jiao, D., Liu, Z.Q., Zhu, Y.K., Weng, Z.Y., Zhang, Z.F., 2016a. Mechanical behavior of mother-of-pearl and pearl with flat and spherical laminations. Mater. Sci. Eng., C 68, 9–17.
Jiao, D., Liu, Z.Q., Qu, R.T., Zhang, Z.F., 2016b. Anisotropic mechanical behaviors and their structural dependences of crossed-lamellar structure in a bivalve shell. Mater. Sci. Eng. C 59, 828–837.
Jones, R.M., 1999. Mechanics of Composite Materials. Taylor & Francis, Philadelphia.
Li, L., Ortiz, C., 2013. Biological design for simultaneous optical transparency and mechanical robustness in the shell of *Placuna placenta*. Adv. Mater. 25, 2344–2350.
Li, L., Weaver, J.C., Ortiz, C., 2015. Hierarchical structural design for fracture resistance in the shell of the pteropod *Clio pyramidata*. Nat. Commun. 6, 6216.
Li, L., Ortiz, C., 2015. A natural 3D interconnected laminated composite with enhanced damage resistance. Adv. Funct. Mater. 25, 3463–3471.
Li, X.D., Chang, W.C., Chao, Y.J., Wang, R.Z., Chang, M., 2004. Nanoscale structural and mechanical characterization of a natural nanocomposite material: the shell of red abalone. Nano Lett. 4, 613–617.
Lin, A.Y.M., Meyers, M.A., Vecchio, K.S., 2006. Mechanical properties and structure of *Strombus gigas*, *Tridacna gigas*, and *Haliotis rufescens* sea shells: a comparative study. Mater. Sci. Eng., C 26, 1380–1389.
Lin, A.Y.M., Chen, P.-Y., Meyers, M.A., 2008. The growth of nacre in the abalone shell. Acta Biomater. 4, 131–138.
Lin, A.Y.M., Meyers, M.A., 2009. Interfacial shear strength in abalone nacre. J. Mech. Behav. Biomed. Mater. 2, 607–612.
Liu, Z.Q., Jiao, D., Zhang, Z.F., 2015. Remarkable shape memory effect of a natural biopolymer in aqueous environment. Biomaterials 65, 13–21.
Liu, Z.Q., Jiao, D., Weng, Z.Y., Zhang, Z.F., 2016. Structure and mechanical behaviors of protective armored pangolin scales and effects of hydration and orientation. J. Mech. Behav. Biomed. Mater. 56, 165–174.
Liu, Z.Q., Zhang, Y.Y., Zhang, M.Y., Tan, G.Q., Zhu, Y.K., Zhang, Z.F., Ritchie, R.O., 2019. Adaptive structural reorientation: developing extraordinary mechanical properties by constrained flexibility in natural materials. Acta Biomater. 86, 96–108.
Liu, Z.Q., Meyers, M.A., Zhang, Z.F., Ritchie, R.O., 2017. Functional gradients and heterogeneities in biological materials: design principles, functions, and bioinspired applications. Prog. Mater Sci. 88, 467–498.
Lopez, M.I., Martinez, P.E.M., Meyers, M.A., 2014. Organic interlamellar layers, mesolayers and mineral nanobridges: contribution to strength in abalone (*Haliotis rufescence*) nacre. Acta Biomater. 10, 2056–2064.
Lopez, M.I., Meyers, M.A., 2016. The organic interlamellar layer in abalone nacre: formation and mechanical response. Mater. Sci. Eng. C 58, 7–13.
Menig, R., Meyers, M.H., Meyers, M.A., Vecchio, K.S., 2000. Quasi-static and dynamic mechanical response of *Haliotis rufescens* (abalone) shells. Acta Mater. 48, 2383–2398.
Meyers, M.A., Chen, P.-Y., Lin, A.Y.M., Seki, Y., 2008a. Biological materials: structure and mechanical properties. Prog. Mater. Sci. 53, 1–206.
Meyers, M.A., Lin, A.Y.M., Chen, P.-Y., Muyco, J., 2008b. Mechanical strength of abalone nacre: role of the soft organic layer. J. Mech. Behav. Biomed. Mater. 1, 76–85.
Meyers, M.A., Lim, C.T., Li, A., Hairul Nizam, B.R., Tan, E.P.S., Seki, Y., McKittrick, J., 2009. The role of organic intertile layer in abalone nacre. Mater. Sci. Eng. C 29, 2398–2410.
Meyers, M.A., Mckittrick, J., Chen, P.-Y., 2013. Structural biological materials: critical mechanics-materials connections. Science 339, 773–779.

Munch, E., Launey, M.E., Alsem, D.H., Saiz, E., Tomsia, A.P., Ritchie, R.O., 2008. Tough, bio-inspired hybrid materials. Science 322, 1516–1520.
Naleway, S.E., Porter, M.M., Mckittrick, J., Meyers, M.A., 2015. Structural design elements in biological materials: application to bioinspiration. Adv. Mater. 27, 5455–5476.
Qu, R.T., Zhang, Z.F., 2013. A universal fracture criterion for high-strength materials. Sci. Rep. 3, 1117.
Qu, R.T., Zhang, Z.J., Zhang, P., Liu, Z.Q., Zhang, Z.F., 2016. Generalized energy failure criterion. Scientific Rep. 6, 23359.
Ritchie, R.O., 2011. The conflicts between strength and toughness. Nat. Mater. 10, 817–822.
Sammis, C.G., Ashby, M.F., 1986. The failure of brittle porous solids under compressive stress states. Acta Metall. 34, 511–526.
Schaffer, T.E., Ionescu-Zanetti, C., Proksch, R., Fritz, M., Walters, D.A., Almqvist, N., Zaremba, C.M., Belcher, A.M., Smith, B.L., Stucky, G.D., Morse, D.E., Hansma, P.K., 1997. Does abalone nacre form by heteroepitaxial nucleation or by growth through mineral bridges? Chem. Mater. 9, 1731–1740.
Song, F., Bai, Y.L., 2003. Effects of nanostructures on the fracture strength of the interfaces in nacre. J. Mater. Res. 18, 1741–1744.
Song, F., Soh, A.K., Bai, Y.L., 2003. Structural and mechanical properties of the organic matrix layers of nacre. Biomaterials 24, 3623–3631.
Sun, J., Bhushan, B., 2012. Hierarchical structure and mechanical properties of nacre: a review. RSC Adv. 2, 7617–7632.
Smith, B.L., Schäffer, T.E., Viani, M., Thompson, J.B., Frederick, N.A., Kindt, J., Belcher, A., Stuckyk, G.D., Morse, D.E., Hansma, P.K., 1999. Molecular mechanistic origin of the toughness of natural adhesives, fibres and composites. Nature 399, 761–763.
Tresca, H., 1864. Sur I' ecoulement des corps solids soumis a defortes pression. Comptes Rendus hebdomadaires des Seancesde I' Academie des Sciences 59, 754–758.
Tsai, S.W., 1968. Strength theories of filamentary structures. In: Schwartz, R.T., Schwartz, H.S. (Eds.), Fundamental Aspects of Fibre Reinforced Plastic Composites. Wiley Interscience, New York, pp. 3–11.
Wang, R.Z., Wen, H.B., Cui, F.Z., Zhang, H.B., Li, H.D., 1995. Observations of damage morphologies in nacre during deformation and fracture. J. Mater. Sci. 30, 2299–2304.
Wang, R.Z., Suo, Z., Evans, A.G., Yao, N., Aksay, I.A., 2001. Deformation mechanisms in nacre. J. Mater. Res. 16, 2485–2493.
Xu, Z.H., Li, X.D., 2011. Deformation strengthening of biopolymer in nacre. Adv. Funct. Mater. 21, 3883–3888.
Yao, N., Epstein, A.K., Liu, W.W., Sauer, F., Yang, N., 2009. Organic–inorganic interfaces and spiral growth in nacre. J. R. Soc. Interface 6, 367–376.
Yin, Z., Hannard, F., Barthelat, F., 2019. Impact-resistant nacre-like transparent materials. Science 364, 1260–1263.
Yourdkhani, M., Pasini, D., Barthelat, F., 2011. Multiscale mechanics and optimization of gastropod shells. J. Bionic Eng. 8, 357–368.
Zhang, Z.F., Eckert, J., 2005. Unified tensile fracture criterion. Phys. Rev. Lett. 94, 094301.
Zheng, B.L., Bai, R., Lei, Z., Yan, C., 2018. Interfacial mechanical behaviour of protein–mineral nanocomposites: a molecular dynamics investigation. J. Biomech. 73, 161–167.